



# Enhanced Corrosion Properties of Nanostructured 316 Stainless Steel in 0.6 M NaCl Solution

Temitope Olugbade<sup>1</sup> · Jian Lu<sup>1,2,3</sup>

Received: 23 October 2018 / Revised: 12 March 2019 / Accepted: 16 March 2019 / Published online: 25 March 2019  
© Springer Nature Switzerland AG 2019

## Abstract

Surface modification through surface mechanical attrition treatment (SMAT) process and annealing were employed to enhance the corrosion properties of 316 stainless steel (SS) in 0.6 M NaCl. SMAT resulted in the formation of a nanocrystalline layer on 316 SS with an average grain size of 20 nm at the depth of about 30  $\mu\text{m}$  from the treated surface. The nanocrystalline microstructure of the surface was characterized by X-ray diffraction and scanning electron microscopy. The micro-hardness of the surface layer of the treated sample was higher than that of the as-received sample by about 100 HV (Vickers hardness) at a depth of 200  $\mu\text{m}$  from the treated surface. By the combined effect of SMAT and low-temperature annealing treatment at 400 °C, the electrochemical tests revealed an improvement in the corrosion properties of 316 SS in terms of corrosion potential and current density. This was attributed to the easy movement of Cr from the material matrix to the surface layer which resulted in the formation of a protective oxide layer on the material surface.

**Keywords** Surface treatment · Annealing · Nanostructure · Corrosion · Oxide layer

## 1 Introduction

AISI 316 stainless steel is widely known for its high strength, durability, and toughness, with applications in most manufacturing industries where excellent corrosion properties and high strength are crucial. Over continuous usage, there is a great tendency for a reduction in strength, beginning at the material surface. Since most material related failures occur on the surface, there is a need to protect and further enhance the strength of the materials using various surface modification techniques. Surface mechanical attrition treatment (SMAT) fits well for this purpose. SMAT is a unique technique for enhancing the mechanical properties and overall

performance of materials without changing their inherent properties [1–3].

As a form of surface nanocrystallization techniques, SMAT has been successfully applied to various material systems including alloys (Mg, Ni, Al), pure iron, titanium, copper, cobalt, intermetallic compound, carbon, and stainless steels [4–20]. It is more efficient than coating and deposition techniques such as physical vapor deposition (PVD) and chemical vapor deposition (CVD) [13, 21]. Over the years, studies on SMAT have been carried out in different forms including the preparation of nanostructured surface layer (grain refinement), characterization of the microstructure, and the mechanical and corrosion properties of materials after treatment. It is important to note that nanostructured materials are characterized by a high-volume fraction of the grain boundary. In addition, there is very high tendency that surface nanocrystallization could influence the corrosion resistance of materials after being subjected to surface treatment [13, 26, 28]. In a recent study [22], the experimental investigations reported a decrease in the protective properties of the passive layer in the nanostructured Cu<sub>89</sub>Ni<sub>09</sub> alloy. In another study [23, 24], the electrochemical characteristics of ultrafine-grained Cu and Ti were reported to be almost the same in comparison with the coarse-grained ones. These findings clearly suggest that the

---

✉ Temitope Olugbade  
tolugbade2-c@my.cityu.edu.hk

<sup>1</sup> Department of Mechanical Engineering, City University of Hong Kong, Hong Kong, China

<sup>2</sup> Department of Material Science and Engineering, Hong Kong Branch of National Precious Metals Material Engineering Research Centre, City University of Hong Kong, Hong Kong, China

<sup>3</sup> Centre for Advanced Structural Materials, Shenzhen Research Institute, City University of Hong Kong, Shenzhen, China

effect of nanocrystallization on corrosion properties varies among materials and alloy systems. Hence, there is still need for an extensive study to deeply investigate and understand the nature of nanocrystallization process and nanocrystalline behavior, especially on the corrosion resistance of stainless steels.

Recently, the corrosion behavior of nanostructured stainless steels using various surface modification techniques has been a subject of investigation. SMAT has been shown to decrease the corrosion resistance of 409 SS at various processing times following the increase in micro-strain during treatment [25]. Compared to the as-received sample, the nanocrystalline 304 SS sample prepared by equal channel angular pressing (ECAP) exhibited a higher corrosion resistance [26]. In addition, Ye [27] observed that the nanocrystalline 309 SS subjected to DC magnetron sputtering presented varying corrosion resistance in different solutions, while surface nanocrystallization of low-carbon steels by SMAT decreased their corrosion resistance [28]. Similarly, Zhang et al. [3] carried out a study on the formation of a nanostructured surface layer on 304 SS by means of SMAT and the effects of the processing parameters on the corrosion resistance.

In this study, AISI 316 SS was the material of choice because of its superior mechanical properties such as hardness and strength, which makes it an ideal material for most petroleum and aerospace industries where excellent corrosion properties are of importance. However, its corrosion resistance can be further enhanced through surface modification by SMAT. The present study focused on the influence of surface modification by SMAT on the corrosion performance of 316 stainless steel. The effect of the processing parameters and the extent of grain refinement on the overall microstructure of the material were investigated. The microstructures of the nanostructured layers were characterized by X-ray diffraction (XRD) and scanning electron microscopy (SEM). To further enhance the corrosion resistance of the nanostructured 316 SS, a low-temperature annealing treatment was carried out.

## 2 Experimental Details

### 2.1 Materials

The material used in the study was a commercial 316 SS with a chemical composition shown in Table 1. Both the as-received sample and the one subjected to SMAT were

cut into sizes ( $70 \times 70 \times 1 \text{ mm}^3$ ) using Electrical Discharge Machine (EDM) (Model: ALN400G, Thailand), and thereafter properly cleaned using acetone before SMAT treatment. The SMAT operation was carried out using the surface nanocrystallization equipment (Model: SNC1, China). The sample subjected to SMAT on both surfaces was treated for 10 min using 2 mm  $\varnothing$  304 SS balls at room temperature. The mass of the ball used was 20 g and the velocity of the ball was in the range of 1–20 m/s. The chamber height and diameter were kept constant at 35 mm and 70 mm, respectively. With the vibrating frequency at 20 Hz, the power amplitude of the electronic signal was adjusted by the generator and kept constant at 80%. The SMAT process has been explained in detail in the literature [3, 18, 19, 29]. The surface profile of the as-received 316 SS sample and the one treated for 10 min was measured using an optical surface profiler (Veeco/Wyko NT9300). After SMAT, a low-temperature annealing treatment was carried out under Argon atmosphere with a flow rate of 20 sccm at 400 °C. The annealing test was completed in a tube furnace with a heating rate of 10 °C/min to the preset temperature, held there for 1 h, and then furnace cooled.

The microstructures of the untreated and treated samples were observed by a Scanning Electron Microscope (FEI Quanta 450 FEG SEM) operating at 20 kV. The chemical composition of the samples' surface layer before and after SMAT was measured using energy dispersive spectroscopy (EDS). X-ray diffraction (XRD) patterns of 316 SS before and after SMAT were measured on D8 Advance X-ray diffractometer (Bruker AXS, USA) using  $\text{Cu K}\alpha$  radiation. The XRD machine operated at 30 kV, 10 mA with the scanning angle between 20° and 100°, at a scanning speed of 10°/min, and step size of 0.02°/s. The average grain size was determined through the full width half maximum (FWHM) of the XRD. The micro-hardness of the untreated and treated samples was measured using Vickers Micro-Hardness Tester (Fischer HM2000XY) at the applied load of 30 g with duration of 20 s on the surface. The loading speed was 50  $\mu\text{m/s}$  with time of application of test force at 10 s while the holding time was 2 s.

### 2.2 Polarization Tests

The corrosion behavior of the as-received sample and the treated one was investigated by electrochemical tests carried out in 0.6 M NaCl solution using Thales Z3.04 USB electrochemical workstation (Model: IM6, ZAHNER elektrik, Germany). It was done using the traditional three-electrode

**Table 1** Chemical composition (wt%) of 316 stainless steel

Elements	C	Si	Mn	Cr	Ni	S	P	Fe
Conc. (wt%)	0.01	0.59	1.19	16.69	10.19	0.01	0.04	Bal

system, with the samples (as-received and treated) as the working electrode, platinum (Pt) as the counter electrode, and Ag/AgCl (stored in KCL solution) as the reference electrode. For the corrosion test, the samples were cut into sizes (20×20×1 mm<sup>3</sup>) and properly cleaned. Only a 10 mm<sup>2</sup> area of the samples (both as-received and treated) was exposed to the electrolyte solution during the test. The electrochemical tests comprised open circuit potential (OCP), potentiodynamic and potentiostatic polarization, and electrochemical impedance spectroscopy (EIS). A cathodic reduction was first carried out at −100 mV (Ag/AgCl) for 900 s to remove any formation of oxide, and then the OCP test was executed to determine the stability of the corrosion potential before the polarization test. After the cathodic reduction, potentiostatic polarization measurement was immediately carried out by determining the level of variation of current with time at OCP. This determined the formation information of the passive film and subsequently determined the level of corrosion resistance of the samples. After the potentiostatic study, potentiodynamic polarization test was carried out to measure the corrosion potential ( $E_{corr}$ ) and corrosion current density ( $i_{corr}$ ) of the as-received and treated samples. The test was completed at a scan rate of 1 mV/s, in the potential range from −100 mV to +120 mV. The EIS study was utilized to compare the impedance behavior difference between the as-received and treated samples, over the frequencies range from 100 MHz to 100 kHz with an amplitude of 10 mV. The electrochemical studies were repeated for three times and the EIS parameters with equivalent circuit models were determined from the Nyquist plot after fitting the data using EIS spectrum analyzer software.

### 3 Results and Discussion

#### 3.1 Characteristics of Untreated and Treated 316 SS

During the SMAT process, there was a repeated multidirectional impingement of the balls on the sample surface leading to grain refinement, which is related to the high density of dislocations. As the ball continuously impacts the material surface, it refines the surface until a nanoscale unit is attained. As shown in Fig. 1a and b, the surface microstructure of the 316 SS sample revealed that SMAT resulted into the formation of nanostructured layer with grain size of about 20 nm. After SMAT, there is a reduction in the grain size of AISI 316 SS and the formation of strain-induced martensite with mechanical twins (as indicated by letter A) in the microstructure image (Fig. 1b). The SEM morphology revealed that severe plastic deformation as well as significant grain refinement occurred on the surface layer of about 30 μm. Compared to the as-received sample with an initial grain size of about 50 μm, the SMATed sample exhibited a

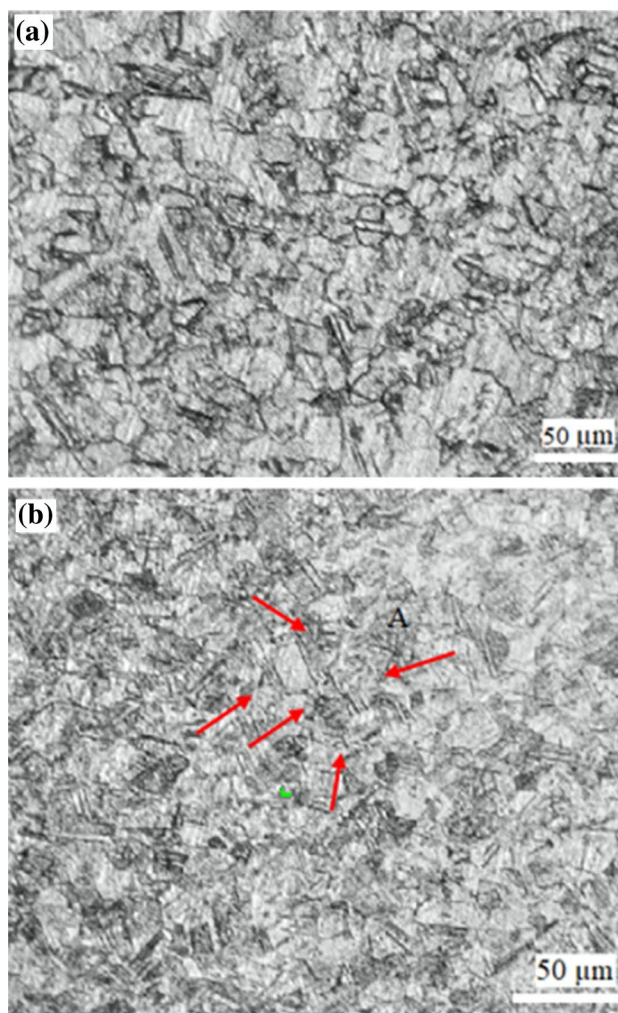


Fig. 1 SEM images of the 316 SS samples: a as-received, b after subjected to SMAT treatment for 10 min, 2 mm Ø 304 SS balls

Table 2 Surface roughness of the as-received and treated 316 SS using 2 mm Ø 304 SS balls

SMAT time (min)	Surface roughness (μm)		
	$R_a$	$R_z$	$R_q$
0	0.43	0.54	0.58
10	0.69	0.42	0.79

grain size of about 20 nm. The grain size of the as-received sample was much larger than the treated sample, and it does change with increasing depth. The microstructural characterization revealed that surface modification by SMAT could fabricate a nanostructured layer on the material surface, reduce the grain size, and form a deformation-induced martensite on the material surface. SMAT increased the surface roughness of the 316 SS sample. The average surface roughness of the as-received and SMATed samples are compiled in Table 2. Compared to the as-received sample with an

average roughness of 0.43  $\mu\text{m}$ , the treated sample exhibited a higher roughness of 0.69  $\mu\text{m}$ , after treatment for 10 min. The increase in surface roughness can be attributed to the formation of scratches and craters following the impact of the balls on the sample surface. However, the extent of increase in surface roughness is a function of treatment time, ball size, ball type, and material property [30–38].

SMAT also improved the hardness of the treated sample with time. The increase in the hardness of the surface layer of the treated sample can be ascribed to the formation of strain-induced martensite and mechanical twins in the material [30]. The hardness of a material is a function of treatment time, vibrating frequency, and operating velocity of the SMAT process. After the SMAT operation, it was observed that the micro-hardness of the surface layer of the treated sample was higher than that of the as-received sample by about 70–110 HV at a depth of 200  $\mu\text{m}$  (Fig. 2).

The XRD patterns of the as-received and treated 316 SS for 10 min using 2 mm  $\varnothing$  balls are shown in Fig. 3. The untreated sample exhibited peaks pertaining to Fe (110), (111), (200), (220), (222), and (321) planes, whereas a little broadening of the peaks pertaining to all the six planes was observed for the treated sample. In addition, the treated sample experienced a higher intensity in the XRD pattern as compared to the as-received one. The width of the XRD peaks was modified by changes in the grain size and the strain induced by the SMAT process. The average grain size on the surface of the SMATed material calculated by FWHM of XRD in the depth range of 0–30  $\mu\text{m}$  was about 20 nm. The SMAT process resulted in high strain and strain rate. The change in grain size was facilitated by the stain induced during treatment, which necessitated the emergence of (110) peak and little broadening of other peaks. In

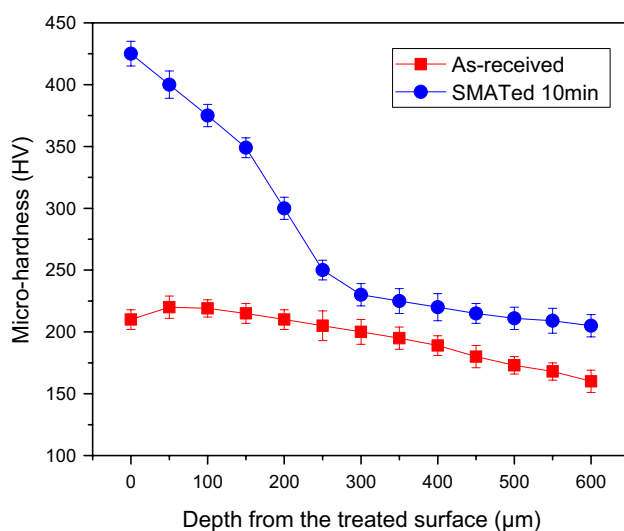


**Fig. 2** Micro-hardness distribution of the as-received and SMATed 316 SS along the depth from the treated surface

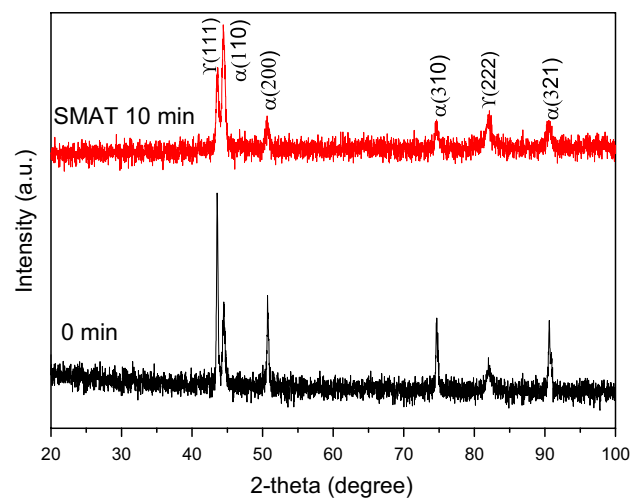


**Fig. 3** XRD patterns of untreated and SMATed 316 SS using 2 mm  $\varnothing$  304 SS balls for 10 min (Color figure online)

addition, there seems to be a phase change after SMAT at  $\gamma$  (111) and  $\alpha$  (110). The broadening of the peaks experienced by the treated sample could be ascribed to the decrease in average grain size on the surface and micro-strain due to dislocations and concentration gradients.

### 3.2 Enhanced Corrosion Behavior of 316 SS

Figure 4 shows the OCP curve of the as-received and treated samples when immersed in 0.6 M NaCl for 30 min. It indicates the relationship between the electrode potential and the immersion time. Compared to the as-received sample, the SMATed sample exhibits an anodic shift with a more positive initial OCP value. Figure 5 shows the potentiodynamic polarization curves of both the as-received and treated

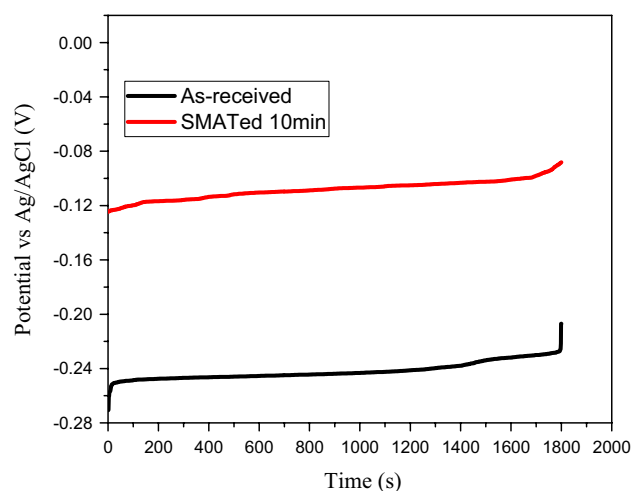


**Fig. 4** OCP curves of the as-received and SMATed 316 SS immersed in 0.6 M NaCl solution for 30 min (Color figure online)

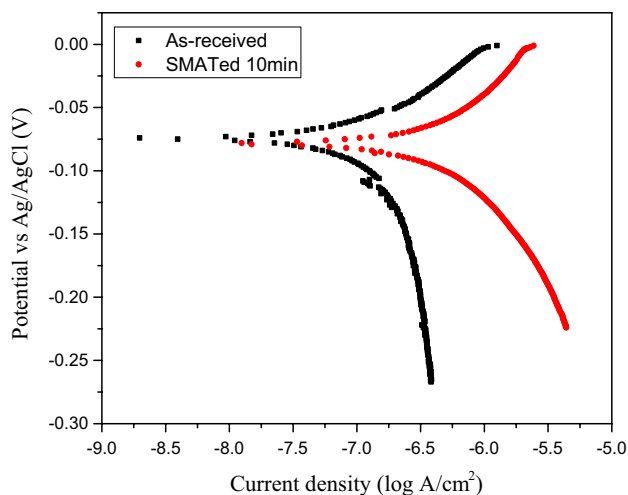


**Fig. 5** Potentiodynamic polarization curve of the as-received and SMATed 316 SS using 2 mm Ø 304 SS balls for 20 min in 0.6 M NaCl solution

samples, in 0.6 M NaCl. The corrosion potentials ( $E_{corr}$ ) and current densities ( $i_{corr}$ ) of the samples, which were obtained from the polarization curves by Tafel extrapolation method, are compiled in Table 3. The polarization studies were repeated for three times and the error values were determined. Compared to the as-received sample, the treated sample exhibited a slight cathodic shift in  $E_{corr}$ . SMAT remarkably changed the polarization behavior of the 316 SS, not only markedly increasing the anodic current density but also slightly lowering the corrosion potential ( $E_{corr}$ ). Compared to the as-received sample, the current–time transients (CTT) recorded at  $-100$  mV (Ag/AgCl) for 900 s clearly shows that the current density of the SMATed sample increased with time (Fig. 6). The surface morphologies of corroded regions of the as-received, SMATed, and annealed samples after polarizing them at  $-100$  mV (Ag/AgCl) for 900 s in 0.6 M NaCl solution at room temperature are shown in Fig. 7. As revealed in Fig. 7a, after the samples were immersed in the solution and polarized for 900 s, intergranular corrosion was observed at the surface layer of the untreated sample. This occurred when a grain boundary area was preferentially attacked due to the presence of precipitates in these areas. As shown in Fig. 7b, the SMATed sample displayed a uniform corrosion caused by hundreds of tiny intergranular

**Table 3** Corrosion parameters of untreated, SMATed, and SMATed + annealed 316 SS samples

Samples	$E_{corr}$ (V)	$I_{corr}$ ( $\mu\text{A}/\text{cm}^2$ )
Untreated	$-0.063 \pm 0.050$	$-6.832 \pm 0.004$
SMATed 10 min	$-0.066 \pm 0.020$	$-6.373 \pm 0.002$
SMAT + annealing	$0.026 \pm 0.010$	$-7.537 \pm 0.001$

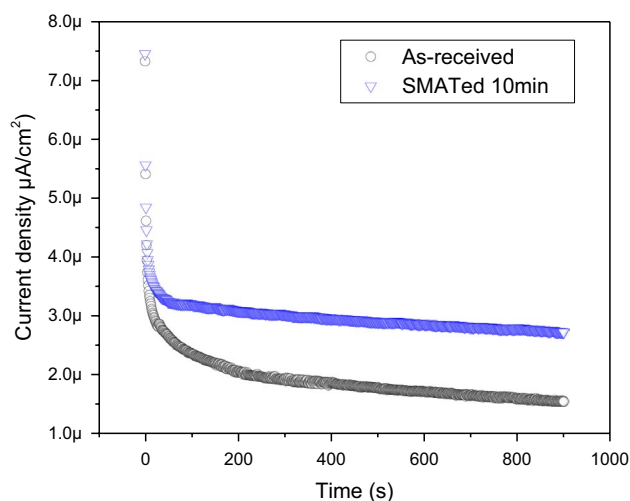


**Fig. 6** Current-time transients of untreated 316 SS and the one subjected to SMAT using 2 mm Ø 304 SS balls for 900 s in 0.6 M NaCl solution at  $-100$  mV

corrosion. After low-temperature annealing, there was a relaxation in the high strain energy induced by the SMAT process, which improves the material surface and subsequently enhanced the corrosion resistance (Fig. 7c and d).

Figure 8 shows the Nyquist, impedance, and phase angle plots of the as-received and treated 316 SS samples in 0.6 M NaCl. The Nyquist plot (Fig. 8a) demonstrates the relationship between the real and imaginary parts of the impedance. Compared to the treated sample with a lower diameter of the semi-circle (Fig. 8a), the as-received sample exhibited a capacitive semi-circle with a much larger diameter in the high-frequency domain obtained from the Nyquist plot. The higher the diameter of the capacitive semi-circle, the higher the film stability and compactness, hence the better the corrosion resistance. The larger diameter of the capacitive semi-circle of the as-received sample implies that more protective passive films had formed on the surface of the treated sample. This shows that there is not much improvement in the corrosion resistance of 316 SS after SMAT. The Bode impedance plot of the as-received and treated samples reveals that the as-received sample experienced an increase in impedance when compared to the SMATed one (Fig. 8b).

Figure 8c shows the phase angle plots of the as-received and treated 316 SS, in which the samples were found in high- and low-frequency ranges. The high angles at low frequencies are the typical feature for passivated materials. From the plot (Fig. 8c), the phase angle maximum of SMATed 316 SS sample is  $61^\circ$ , whereas the as-received sample exhibits a higher phase angle maximum of  $68^\circ$ . The increase in the phase angle maximum observed for the as-received sample is due to the formation of a compact passive film at the surface. The decrease in phase angle maximum depicts the formation of a porous film on the

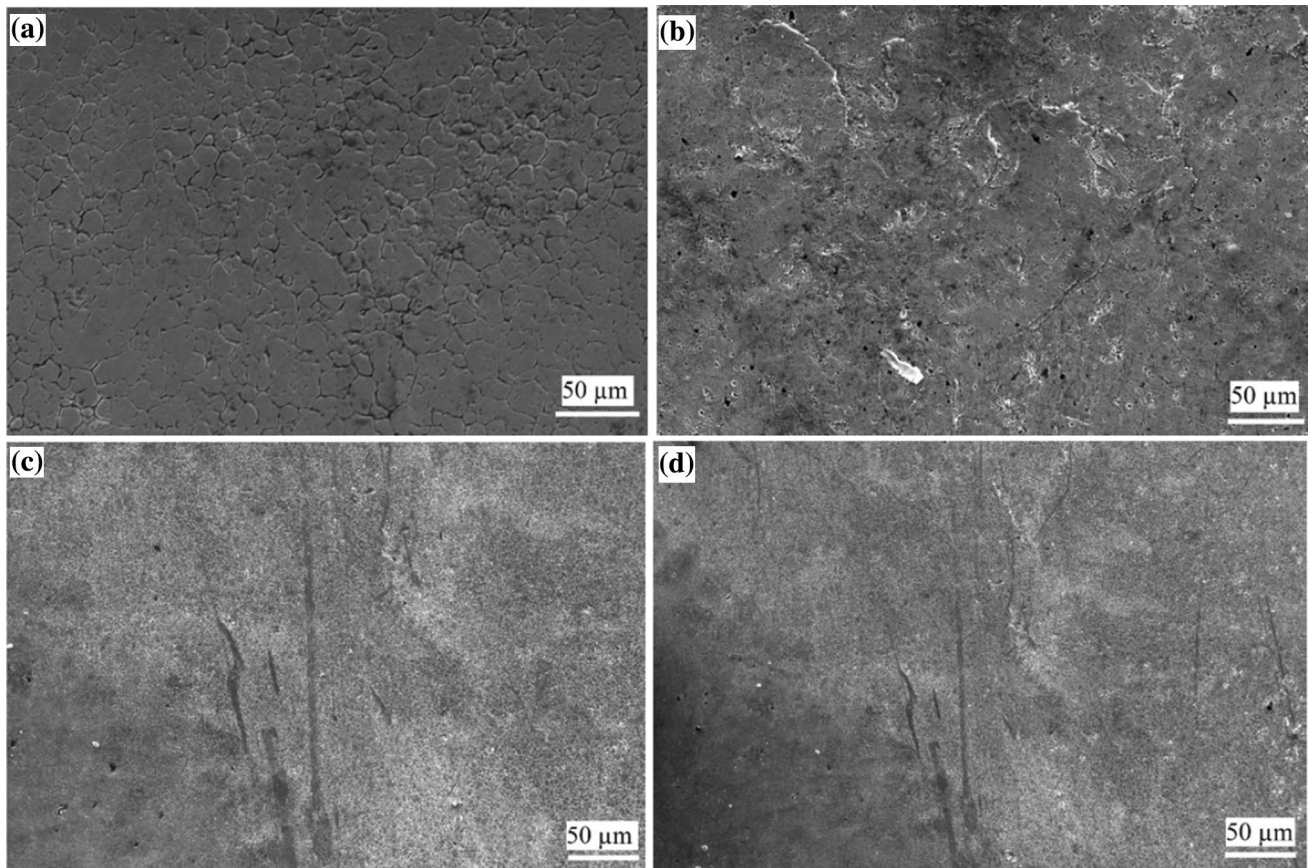
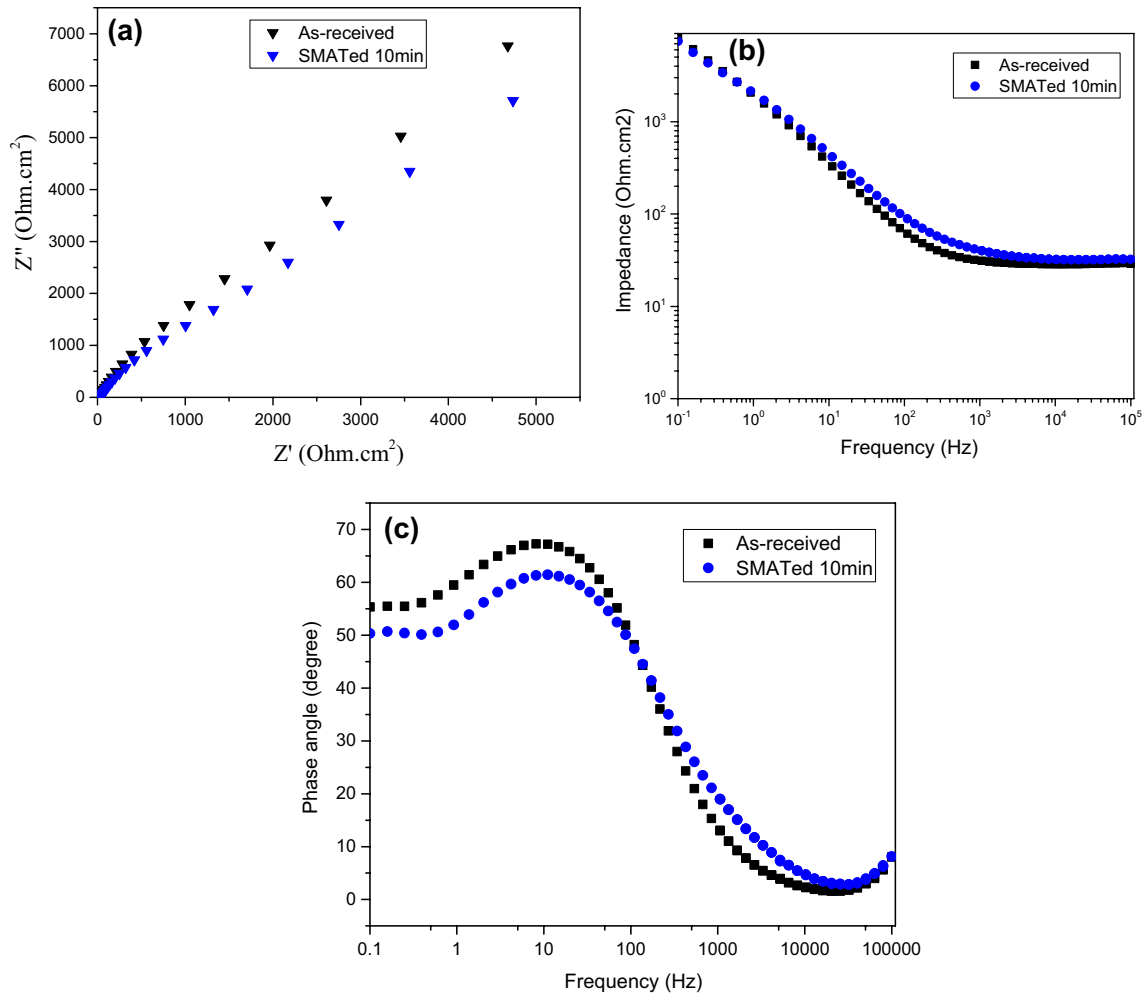


**Fig. 7** Surface morphology of 316 SS samples after polarizing them from  $-100$  to  $+120$  mV<sub>(Ag/AgCl)</sub> from their respective open circuit potentials in 0.6 M NaCl solution: **a** untreated; **b** SMATed sample; **c** and **d** SMATed + annealed samples at 400 °C for 1 h

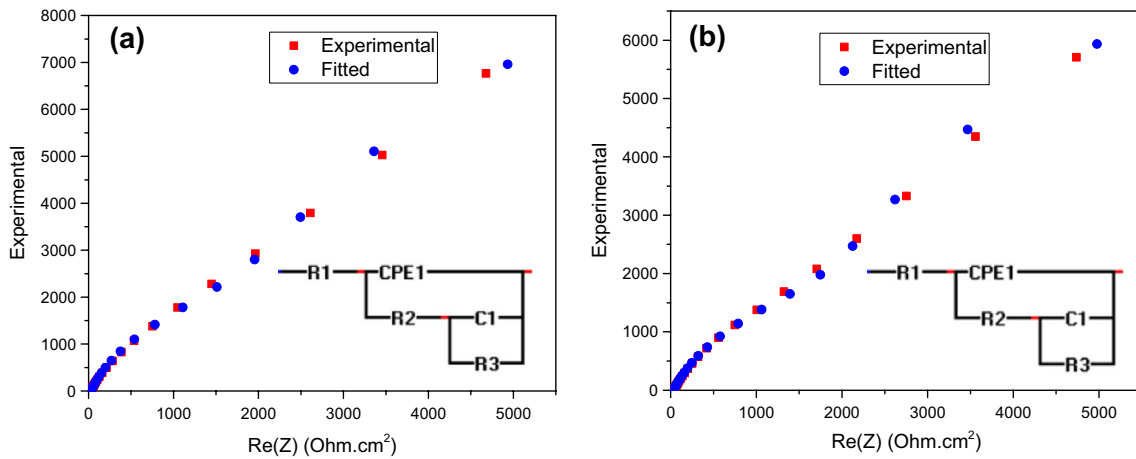
surface of treated sample. The  $\chi^2$  goodness of fit test was used to analyze the EIS data and obtain the best fit. For all the samples, the fittings obtained for the EIS data along with the corresponding equivalent electrical circuit models are shown in Fig. 9. In these models, R represents the solution resistance, C represents the capacitances, whereas CPE represents the constant phase element. The validity of the models is confirmed based on the better non-linear least square fitting of the experimental data within 5% error. The EIS data were approximated using different electronic equivalent circuits built in EIS spectra analyzer software, and the best fit was obtained. The EIS parameters of the as-received and treated samples are compiled in Table 4 with Chi-square goodness of fit values of 0.003 and 0.010 for the untreated and SMATed samples, respectively. Compared to the as-received 316 SS, the SMATed sample exhibited a decrease in resistance. Figure 10 shows the double-log plots for potentiostatic polarization of the as-received and treated 316 SS samples at OCP in 0.6 M NaCl solution. The corrosion behaviors of the as-received and treated samples observed by OCP (Fig. 4), potentiodynamic polarization (Fig. 5 and Table 3), current–time

transient's analysis (Fig. 6), and EIS studies (Fig. 8 and Table 4) corroborate with each other.

To relax the residual stress and release the high strain energy induced during SMAT, the treated 316 SS sample was subjected to a low-temperature annealing treatment at 400 °C for 1 h. It is important to note that nanocrystalline grows on the material surface after annealing treatment and the nanostructured layer was observed to remain stable at 400 °C. The resulting potentiodynamic polarization curve is shown in Fig. 11a and b. The corrosion potential ( $E_{\text{corr}}$ ) significantly increased from  $-0.063 \pm 0.050$  V to  $0.026 \pm 0.010$  V, while the corrosion current density ( $i_{\text{corr}}$ ) decreased from  $-6.832 \pm 0.004$   $\mu\text{A}/\text{cm}^2$  to  $-7.537 \pm 0.001$   $\mu\text{A}/\text{cm}^2$ . The polarization results indicate that the corrosion resistance of the nanostructured 316 SS has improved significantly after surface modification by SMAT and low-temperature annealing treatment. As shown in Fig. 12a and b, the XPS results showed a higher concentration of Cr in the passive layer on the sample surface after SMAT and annealing processes. Compared with the as-received sample, the SMATed and annealed samples experienced a rapid migration of Cr from the bulk (at about 400–800 nm) to the surface (about



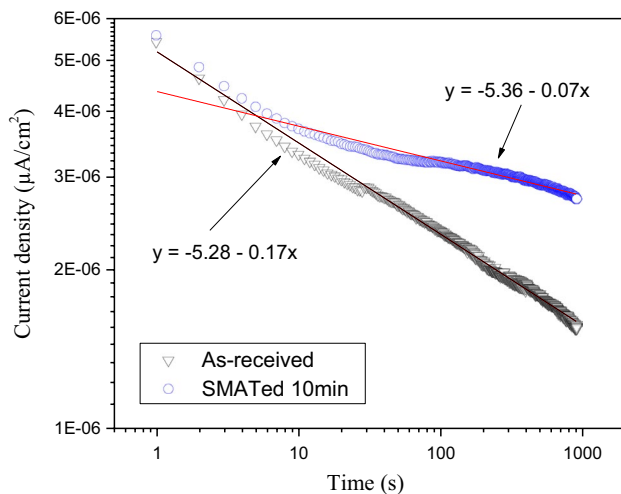
**Fig. 8** The Nyquist **a** Bode impedance **b** and Bode phase angle **c** plots of untreated AISI 316 SS and samples SMATed using 2 mm  $\varnothing$  304 SS balls for 10 min in 0.6 M NaCl



**Fig. 9** Non-linear least square fitting obtained for the EIS data along with the corresponding equivalent electrical circuit model of untreated and SMATed 316 SS using 2 mm  $\varnothing$  304 SS balls: **a** untreated; **b** SMATed for 10 min

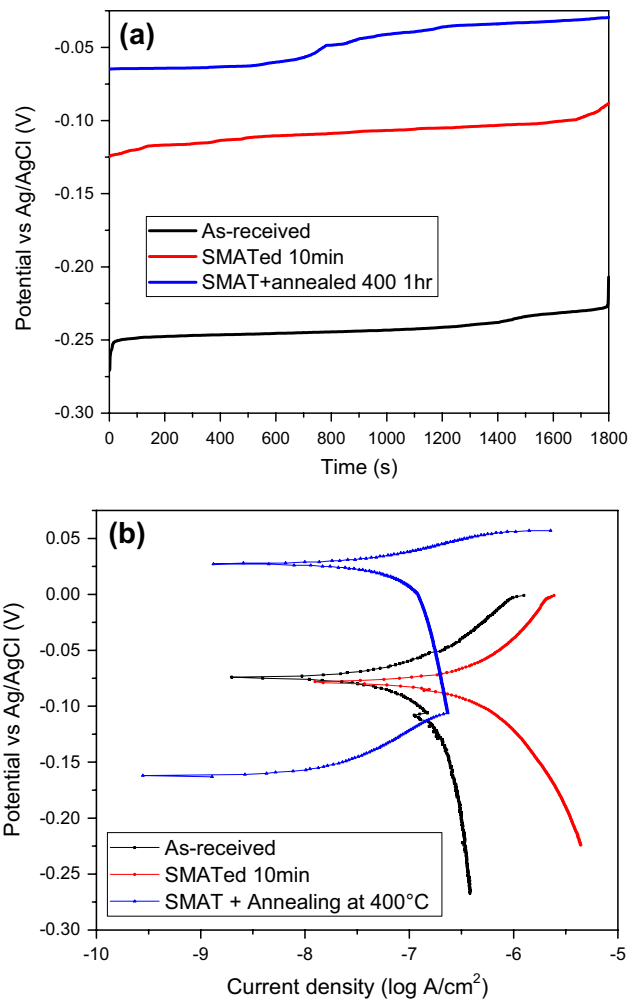
**Table 4** EIS parameters of untreated and SMATed 316 SS using 2 mm Ø 304 SS balls in 0.6 M NaCl at their respective OCPs

S/N	EIS parameters	Untreated	SMATed
1	$R_1$ (Ohm $\text{cm}^2$ )	$29.175 \pm 1.091$	$33.799 \pm 1.428$
2	$R_2$ ( $\times 10^4$ Ohm $\text{cm}^2$ )	$0.592 \pm 1.965$	$0.483 \pm 2.864$
3	$\text{CPE}_1$ ( $\times 10^{-5}$ F $\text{cm}^{-2}$ )	$8.690 \pm 2.938$	$8.260 \pm 6.709$
4	$n_1$	$0.850 \pm 0.632$	$0.790 \pm 1.374$
5	$R_3$ ( $\times 10^4$ Ohm $\text{cm}^2$ )	$1.884 \pm 8.864$	$1.517 \pm 1.667$
6	$C_1$ ( $\times 10^{-4}$ F)	$1.190 \pm 2.985$	$1.380 \pm 4.826$
7	$\chi^2$ goodness of fit values	0.003	0.010

**Fig. 10** Current versus time plots of untreated and SMATed 316 SS using 2 mm Ø 304 SS balls for 900 s recorded at  $-100$  mV (Ag/AgCl) in 0.6 M NaCl

0–250 nm). In addition, the combined effects of SMAT and annealing significantly increased the signal intensity of  $\text{Cr}_2\text{O}_3$  at the binding energy of 530.5 eV, as shown in Fig. 12b. Due to the low-temperature annealing treatment, there was a relaxation of the residual stress and the high strain energy stored was relieved. This helped in the formation of nucleation sites through which Cr can easily move to the material surface (Fig. 12a), hence forming a protective oxide layer. Figure 13 shows the atomic percentage of the passive films and the sputter depth of untreated, SMATed, and annealed 316 SS samples. Besides the presence of Fe2p, Cr2p, O1s, and Ni2p3 in the as-received sample, other elements such as Mn2p and Cl2p were also identified in the SMAT and annealed samples.

In the present study, the combined effect of SMAT using 2 mm Ø balls for 10 min and low-temperature annealing at  $400^\circ\text{C}$  significantly enhanced the corrosion resistance of 316 SS in 0.6 M NaCl solution (Table 3 and Fig. 11). The surface nanocrystallization by SMAT using 2 mm for 900 s also increased the corrosion resistance of 409 SS sample in

**Fig. 11** Electrochemical test results after SMAT and low-temperature annealing at  $400^\circ\text{C}$ . **a** OCP curves of the as-received, SMATed, and annealed samples, **b** polarization curves of the as-received, SMATed, SMATed + annealed samples (Color figure online)

0.6 M NaCl [25]. The improvement in corrosion resistance was attributed to surface nanocrystallization which enabled an enhanced diffusion of Cr and improved the passivation ability. The corrosion resistance of AZ91D Mg alloy in 0.6 M NaCl was also improved through surface nanocrystallization by SMAT using 2 mm Ø balls for 1800 s [39]. Hence, surface nanocrystallization combined with low-temperature annealing could enhance the passivation ability and improve the corrosion resistance of materials.

## 4 Conclusion

In the present study, the surface nanocrystallization of 316SS sample had been achieved by fabricating a nanostructured surface layer (grain size of 20 nm at the depth of about  $30\ \mu\text{m}$  from the treated surface) on the material



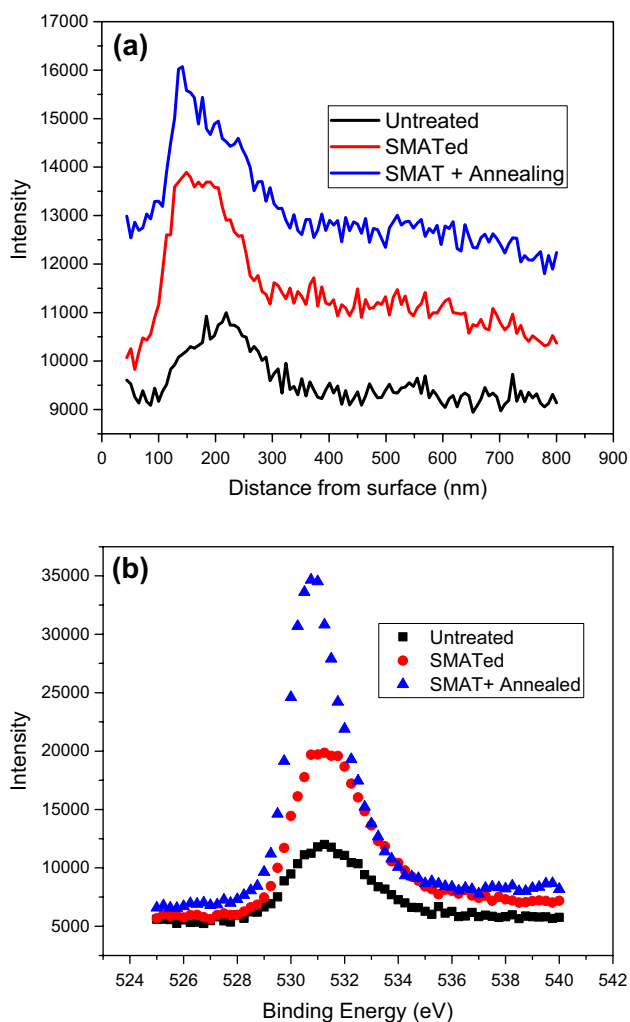


**Fig. 12** XPS analysis of untreated, SMATed, and SMATed + annealed 316 SS samples **a** Cr concentration depth profile, **b** Cr 2p core-level spectra showing the intensity at different binding energy levels (Color figure online)

surface through SMAT. The nanocrystalline microstructure of the surface induced by SMAT was characterized by scanning electron microscopy (SEM) and X-ray diffraction (XRD). At a depth of 200 μm from the treated surface, the micro-hardness of the treated sample improved from 215 to 310 HV after SMAT. By the combined effect of SMAT and low-temperature annealing treatment, the electrochemical tests revealed an improvement in the corrosion resistance of 316 SS. This was attributed to the quick formation of a protective dense oxide layer on the material surface through the diffusion of Cr from the matrix to the surface layer. It can be concluded that the corrosion resistance of SMATed 316 SS in 0.6 M NaCl depends on the extent of nanocrystallization and strain induced during treatment. The nanostructured 316 SS with an enhanced corrosion resistance will find application in most automotive and manufacturing industries.

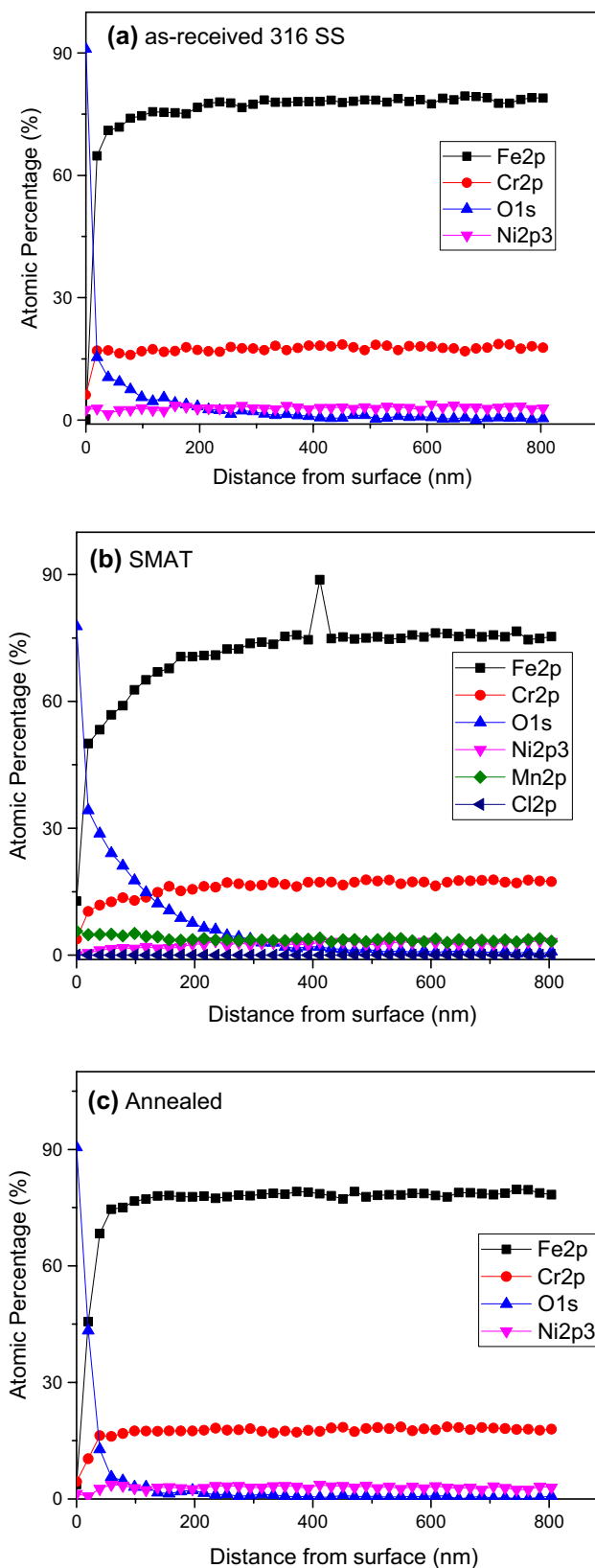


**Fig. 13** XPS analysis—atomic percentage of the passive films on 316 SS samples after corrosion test in natural condition as a function of sputter depth (Fe2p, Cr2p, O1s, Mn2p, Ni2p3, Cl2p): **a** as-received, **b** SMATed and, **c** SMATed + annealed samples

**Acknowledgements** Professor J. Lu acknowledges the supports of the National Key R&D Program of China (Project No. 2017YFA0204403) and the Major Program of National Natural Science Foundation of China: NSFC 51590892. This work was also supported by the Government of Hong Kong, Hong Kong SAR, China, Hong Kong (PF16-02783). T. Olugbade appreciates the efforts of Dr Chan Lap Chung and Dr Liu Chang (City University of Hong Kong) for their assistance in the SMAT process and corrosion test, respectively.

## Compliance with Ethical Standards

**Conflict of interest** The authors report no conflict of interest.

## References

- Tao NR, Wang ZB, Tong WP, Sui ML, Lu J, Lu K (2002) An investigation of surface nanocrystallization mechanism in Fe induced by surface mechanical attrition treatment. *Acta Mater* 50:4603–4616
- Zhu KY, Vassel A, Brisset F, Lu K, Lu J (2004) Nanostructure formation mechanism of  $\alpha$ -titanium using SMAT. *Acta Mater* 52:4101–4110
- Zhang HW, Hei ZK, Liu G, Lu J, Lu K (2003) Formation of nanostructured surface layer on AISI 304 stainless steel by means of surface mechanical attrition treatment. *Acta Mater* 51:1871
- Wang ZB, Tao NR, Li S, Wang W, Liu G, Lu J, Lu K (2003) Effect of surface nanocrystallization on friction and wear properties in low carbon steel. *Mater Sci Eng A* 352:144–149
- Tao NR, Sui ML, Lu J, Lu K (1999) Surface nanocrystallization of iron induced by ultrasonic shot peening. *Nanostruct Mater* 11:433
- Zhang L, Han Y (2010) Effect of nanostructured titanium on anodization growth of self-organized TiO<sub>2</sub> nanotubes. *Nanotechnology* 21:055602
- Wang K, Tao NR, Liu G, Lu J, Lu K (2006) Plastic strain-induced grain refinement at the nanometer scale in copper. *Acta Mater* 54:5281
- Wu X, Tao N, Hong Y, Liu G, Xu B, Lu J, Lu K (2005) Strain-induced grain refinement of cobalt during surface mechanical attrition treatment. *Acta Mater* 53:681
- Wu X, Tao N, Hong Y, Lu J, Lu K (2005) Localized solid-state amorphization at grain boundaries in a nanocrystalline Al solid solution subjected to surface mechanical attrition. *J Phys D* 38:4140–4143
- Chang HW, Kelly PM, Shi YN, Zhang MX (2012) Thermal stability of nanocrystallized surface produced by surface mechanical attrition treatment in aluminum alloys. *Surf Coat Technol* 206:3970–3980
- Wu X, Tao N, Hong Y, Xu B, Lu J, Lu K (2002) Microstructure and evolution of mechanically-induced ultrafine grain in surface layer of AL-alloy subjected to USSP. *Acta Mater* 50:2075
- Chen AY, Ruan HH, Wang J, Chan HL, Wang Q, Li Q, Lu J (2011) The influence of strain rate on the microstructure transition of 304 stainless steel. *Acta Mater* 59:3697–3709
- Dang C, Olugbade TO, Fan S, Zhang H, Gao LL, Li J, Lu Y (2018) Direct quantification of mechanical responses of TiSiN/Ag multilayer coatings through uniaxial compression of micropillars. *Vacuum* 156:310–316
- Lin Y, Lu J, Wang L, Xu T, Xue Q (2006) Surface nanocrystallization by surface mechanical attrition treatment and its effect on structure and properties of plasma nitrided AISI 321 stainless steel. *Acta Mater* 54:5599
- Tao NR, Wu XL, Sui ML, Lu J, Lu K (2004) Grain refinement at the nanoscale via mechanical twinning and dislocation interaction in a nickel-based alloy. *J Mater Res* 19:1623
- Tao NR, Zhang HW, Lu J, Lu K (2003) Development of nanostructures in metallic materials with low stacking fault energies during surface mechanical attrition treatment (SMAT). *Mater Trans* 44:1919
- Sun HQ, Shi YN, Zhang MX, Lu K (2007) Plastic strain-induced grain refinement in the nanometer scale in Mg alloy. *Acta Mater* 55:975
- Tao NR, Lu J, Lu K (2008) Surface nanocrystallization by surface mechanical attrition treatment. *Mater Sci Forum* 579:91–108
- Ren JW, Shan AD, Zhang JB, Song HW, Liu JL (2006) Surface nanocrystallization of Ni<sub>3</sub>Al by surface mechanical attrition treatment. *Mater Lett* 60:2076–2079
- Balusamy T, Sankara Narayanan TSN, Ravichandran K (2012) Effect of surface mechanical attrition treatment (SMAT) on boronizing of EN8 steel. *Surf Coat Technol* 213:221–228
- Dang C, Yao Y, Olugbade TO, Li J, Wang L (2018) Effect of multi-interfacial structure on fracture resistance of composite TiSiN/Ag/TiSiN multilayer coating. *Thin Solid Films* 653:107–112
- Barbucci A, Faroe G, Matteazzi P et al (1999) Corrosion behaviour of nanocrystalline Cu90Ni10 alloy in neutral solution containing chlorides. *Corros Sci* 41:463
- Vinogradov A, Mimaki T, Hashimoto S et al (1999) On the corrosion behaviour of ultra-fine grain copper. *Scr Mater* 41:319
- Balyanov A, Kutnyakova J, Amirkhanova NA et al (2004) Corrosion resistance of ultra fine-grained Ti. *Scr Mater* 51:225
- Balusamy T, Kumar S, Sankara Narayanan TSN (2010) Effect of surface nanocrystallization on the corrosion behavior of AISI 409 stainless steel. *Corros Sci* 52:3826–3834
- Zheng ZJ, Gao Y, Gui Y, Zhu M (2012) Corrosion behaviour of nanocrystalline 304 stainless steel prepared by equal channel angular pressing. *Corros Sci* 54:60–67
- Ye W, Li Y, Wang FH (2006) Effect of nanocrystallization on the corrosion behavior of 309 stainless steel. *Electrochim Acta* 51:4426–4432
- Li Y, Fang F, Liu G (2004) Grain size effect on the electrochemical corrosion behavior of surface nanocrystallized low-carbon steel. *Corrosion* 60:891–896
- Arifvianto B, Mahardika SM (2012) Effects of surface mechanical attrition treatment (SMAT) on a rough surface of AISI 316L stainless steel. *Appl Surf Sci* 258:4538–4543
- Kwok CT, Cheng FT, Man HC, Ding WH (2006) Corrosion characteristics of nanostructured layer on 316 l stainless steel fabricated by cavitation-annealing. *Mater Lett* 60:2419–2422
- Kikuchi S, Komotori J (2010) Properties of gas nitrided austenitic stainless steel pre-treated with fine particle peening. *Int J Fatigue* 32:403–410
- Mahagaonkar SB, Brahmankar PK, Seemikeri CY (2009) Effect on fatigue performance of shot peened components: an analysis using DOE technique. *Int J Fatigue* 31:693–702
- Dai K, Villegas J, Stone Z, Shaw L (2004) Finite element modeling of the surface roughness of 5052 Al alloy subjected to a surface severe plastic deformation process. *Acta Mater* 52:5771–5782
- Abioye TE, Olugbade TO, Ogedengbe TI (2017) Welding of dissimilar metals using gas metal arc and laser welding techniques: a review. *J Emerg Trends Eng Appl Sci* 8:225–228
- Ogedengbe T, Olugbade TO, Olagunju O (2015) Application of house of quality matrix to material selection for engineering designs. *Br J Appl Sci Technol* 10:1–11
- Liu G, Lu J, Lu K (2000) Surface nanocrystallization of 316L stainless steel induced by ultrasonic shot peening. *Mater Sci Eng A* 286:91–95

37. Anand Kumar S, Ganesh S, Sankara Narayanan TSN, Gnana-moorthy R (2012) Fretting wear behaviour of surface mechanical attrition treated alloy 718. *Surf Coat Technol* 206:4425–4432
38. Arifvianto B, Suyitno M, Mahardika P, Dewo PT, Iswanto UA (2011) Effect of surface mechanical attrition treatments (SMAT) on microhardness, surface roughness, and wettability of AISI 316L. *Mater Chem Phys* 125:418–426
39. Laleh M, Kargar F (2011) Effect of surface nanocrystallization on the microstructural and corrosion characteristics of AZ91D magnesium alloy. *J Alloys Compd.* 509:9150–9156